Rapid Communications

Pseudo-icosahedral $Cr_{55}Al_{232-\delta}$ as a high-temperature protective material

R. Rosa,[1] S. Bhattacharya,[2] J. Pabla,[1] H. He,[3] J. Misuraca,[4] Y. Nakajima,[4] A. D. Bender,[1] A. K. Antonacci,[1] W. Adrip,[1] D. E. McNally,[5] A. Zebro,[5] P. Kamenov,[5] G. Geschwind,[5] S. Ghose,[6] E. Dooryhee,[6] A. Ibrahim,[7] T. M. Tritt,[2] M. C. Aronson,[3] and J. W. Simonson[1,*]

[1]*Department of Physics, Farmingdale State College, Farmingdale, New York 11735, USA*
[2]*Department of Physics and Astronomy, Clemson University, Clemson, South Carolina 29634, USA*
[3]*Department of Physics and Astronomy, Texas A&M University, College Station, Texas 77843, USA*
[4]*JEOL USA Incorporated, 11 Dearborn Road, Peabody, Massachusetts 01960, USA*
[5]*Department of Physics and Astronomy, Stony Brook University, Stony Brook, New York 11794, USA*
[6]*National Synchrotron Light Source II, Brookhaven National Laboratory, Upton, New York 11973, USA*
[7]*Department of Mechanical Engineering Technology, Farmingdale State College, Farmingdale, New York 11735, USA*

(Received 16 November 2017; published 19 March 2018)

We report here a course of basic research into the potential suitability of a pseudo-icosahedral Cr aluminide as a material for high-temperature protective coatings. $Cr_{55}Al_{232-\delta}$ [$\delta = 2.70(6)$] exhibits high hardness at room temperature as well as low thermal conductivity and excellent oxidation resistance at 973 K, with an oxidation rate comparable to those of softer, denser benchmark materials. The origin of these promising properties can be traced to competing long-range and short-range symmetries within the pseudo-icosahedral crystal structure, suggesting new criteria for future materials research.

DOI: 10.1103/PhysRevMaterials.2.032401

Given their low cost and abundance, it is expected that coal, natural gas, and other fossil-based energy sources will remain the dominant fuels for global electrical power generation for the coming decades, even as fossil fuel-burning plants emit a wide range of pollutants, including SO_x, NO_x, particulate matter, and most notably CO_2, a widely recognized greenhouse gas [1]. The efficiency of turbine-based power generation is predominantly determined by steam temperature, which is currently limited by the maximum service temperature of exposed steel components [2]. To this end, advances in the fabrication of creep-resistant, high-strength steels over the course of the last decade [3–5]—largely the result of solid solution strengthening via compositional tuning [6,7] together with microstructural control through grain boundary pinning [5,8,9]—have resulted in alloys capable of long-term structural stability to temperatures as high as 973 K. The typically low (∼10%) Cr content of these alloys limits their oxidation resistances, however, necessitating the development of suitable protective coatings to inure exposed components to corrosion, wear, and oxidation under consistently harsh operating conditions [10].

Prospective coating materials must meet critical economic considerations such as ease of fabrication and low cost, in addition to exhibiting desired functionality, including high hardness, low thermal conductivity, low density, and substantial resistance to oxidation [11]. Accordingly, proposed coatings often contain Cr and Al, in part due to the low mass and relative abundance of these elements, but most critically because their oxides often form protective scales, which arrest the diffusion of oxygen from penetrating deeper into coated components. Due to the high chemical stability of Al_2O_3 in particular, attempts to aluminize creep-resistant steels have received significant attention [12,13], but it has proven challenging to impede undesirable chemical interdiffusion between aluminide surfaces and Fe-rich bulks [14,15]. On the other hand, Cr-rich phases have been observed to act as diffusion barriers [16,17], and substantial work has been done in the hopes of impeding compositional diffusion by introducing Cr to Al-rich coatings and thereby triggering the *in situ* growth of Cr_5Al_8 or Cr_2Al layers in response to heat treatment [18–20]. An entirely new triclinic binary compound Cr_4Al_{11} [21] was recently discovered while heat treating Al/Cr composite films [22], suggesting that basic research into this class of materials is far from complete.

We present here the synthesis, hardness, thermal conductivity, and oxidation resistance of high-quality single crystals of $Cr_{55}Al_{232-\delta}$ [$\delta = 2.70(6)$], a previously uninvestigated binary compound that appears well suited to coating applications. This compound was first reported in studies of phase equilibria some 25 years ago as μ-$CrAl_4$ [23]. Motivated by reports that the properties of oxidation-resistant coatings are often strongly influenced by deposition methods [24], we synthesized $Cr_{55}Al_{232-\delta}$ in single-crystal form. Single crystals permit direct measurement of intrinsic properties independent from deposition techniques and free from grain boundaries and impurities, which may be prevalent in samples synthesized via traditional polycrystalline routes. We discuss these properties in terms of the pseudo-icosahedral μ-$MnAl_4$ structure [25,26] adopted by this compound [23,27,28]. We observe low thermal conductivity, likely a direct consequence of the complex crystallographic unit cell. Nearest-neighbor Cr-Al distances measure 2.5 Å or less for all Cr positions, suggesting strong Cr-Al hybridization, which our measurements of high

*jack.simonson@farmingdale.edu

hardness and modest fracture toughness imply is predominantly covalent in character. Further, we observe the formation of a robust Al_2O_3 protective scale upon heat treatment at 973 K. Taken together, these results suggest that $Cr_{55}Al_{232-\delta}$ and related materials have promise as high-temperature coatings.

We grew high-quality single crystals of $Cr_{55}Al_{232-\delta}$ as large as 300 mm^3 by a self-flux technique in which elemental precursors with an initial Cr:Al ratio of 15:85 were sealed under Ar gas, heated to 1303 K, and slowly cooled to 1213 K over 90 h. We determined the structure of the resulting crystals using an Oxford Gemini single-crystal diffractometer with Mo $K\alpha$ radiation, with greater detail presented in the Supplemental Material (SM) [29]. Polycrystalline samples were produced by grinding single crystals to a powder, followed by cold pressing and sintering to a pellet of 70% theoretical density.

We measured thermal conductivity via the steady state technique using a custom-built apparatus [30], and we carried out thermal diffusivity measurements with a NETZSCH LFA-457. Vickers microhardness and fracture toughness measurements were performed with a Mitutoyo digital microhardness tester. We characterized the formation of oxide scale by scanning electron microscopy (SEM) and energy dispersive x-ray spectroscopy (EDX) carried out on a JEOL 7600F Analytical SEM. A cross section was prepared in a JEOL IB-19500CP broad Ar ion beam polisher for 5 h at 8 kV. Images of the cross section were acquired using a JEOL 7200F FE-SEM. We quantified oxidative mass increase by removing the sample from a 973 K furnace, quenching it in air, measuring the mass via precision balance, and reinserting it directly into the 973 K furnace for rapid rethermalization, a process repeated for each subsequent measurement. We carried out diffraction measurements from 300 to 973 K by heating powderized single crystals *in situ* via a quadruple lamp furnace [31] on the X-ray Powder Diffraction (XPD) beamline (28ID-2) at the National Synchrotron Light Source II, Brookhaven National Laboratory. The energy of the incident x rays was 68 keV.

The crystal structure of $Cr_{55}Al_{232-\delta}$ is dominated by pseudo-icosahedral substructures. Figure 1(a) shows the unit cell and an arbitrary selection of representative coordination polyhedra that span the cell. Overall, nine of the ten Cr positions are icosahedrally coordinated, as are three of the Al atomic sites as previously reported [28]. The large unit cell parameters $a = 20.1804(3)$ Å and $c = 24.8530(4)$ Å result directly from local proximity to icosahedral symmetry, which is fundamentally incompatible with periodicity. We observe that the Al(32) site is approximately half occupied, as was also observed in the Mn-based analog, yielding a composition of $Cr_{55}Al_{232-\delta}$ with $\delta = 2.70(6)$. Two neighboring Al(32) sites are located only 1.705(9) Å from one another, with this unphysically short distance indicating that only one of each pair can be occupied. While partial occupancy was previously observed on the Al7 site in the Cr-based system [28], we see no evidence of less than full occupancy in our crystals, indicating that $Cr_{55}Al_{232-\delta}$ exists over a range of δ.

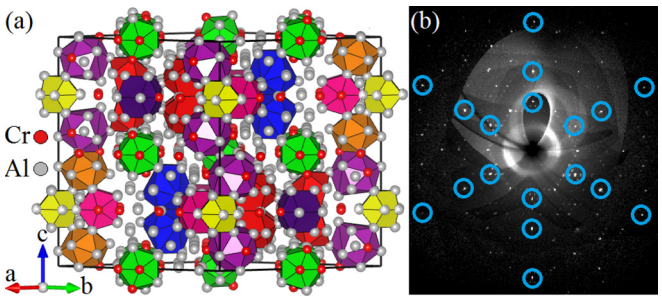

FIG. 1. (a) The unit cell of $Cr_{55}Al_{232-\delta}$ with Cr atoms (red) and Al atoms (gray), as indicated. Representative coordination polyhedra are approximately icosahedral and colored as follows: Cr8 (red), Cr5 (orange), Cr9 (yellow), Al4 (green), Al9 (blue), Al2 (indigo), Al24 (violet), Al16 (pink). Complete crystallographic details are included as Supplemental Material. (b) The ($hk0$) reciprocal space map showing sixfold rotational symmetry. Blue circles highlight bright spots with wave-vector Q ratios that are integral approximates of those expected for an icosahedral quasicrystal (see text).

This complex structure is characterized by the interplay between short-range pseudo-icosahedral symmetry and long-range hexagonal symmetry, as reflected in reciprocal space maps, such as the ($hk0$) plane shown in Fig. 1(b). Overall, we observe that the reflections are circular and sharp, attesting to the high quality of our crystals. The sixfold rotational symmetry associated with space group $P6_3/mmc$ is evident, but closer inspection of the Laue spot intensities reveals that icosahedral symmetry coexists at short length scales within the long-range order. In icosahedral quasicrystals, the ratios between the magnitudes of scattering vectors Q_i for discrete Laue spots i are given by the golden ratio $\tau = (1+\sqrt{5})/2 \simeq 1.618$ [32]. For pseudo-icosahedral crystals, however, bright integral Bragg spots associated with long-range periodicity instead preserve the golden ratio in approximation when $i = (2,3,5,8,13,\ldots)$, yielding $3/2 \simeq 5/3 \simeq 8/5 \simeq 13/8 \simeq \tau$. Accordingly, even though $Cr_{55}Al_{232-\delta}$ is truly crystalline and therefore exhibits long-range periodicity, we still observe the signature of local icosahedral symmetry along, for instance, the (210) and symmetry-equivalent directions. The indicated bright spots are indexed as $(\pm 2i \ \pm i \ 0)$, where $i = 5$, 8, 13, as would be expected. Interestingly, this pattern does not persist to $i < 5$, indicating that icosahedral symmetry does not extend to length scales beyond 3 Å, in excellent agreement with the extent of the icosahedra in our structural model.

Our crystallographic analysis finds that $Cr_{55}Al_{232-\delta}$ is both lightweight and strong. The refined composition and lattice parameters yield a density of only 3.43 g/cm^3, merely 27% greater than that of elemental Al. Nonetheless, the Cr-Al nearest-neighbor distances are invariably short, ranging from 2.4617(9) to 2.506(3) Å for each Cr position—while those reported in other Cr-Al binary compounds such as Cr_5Al_8 or Cr_2Al are without exception longer than 2.6 Å [33,34]—suggesting that Cr-Al bonding in $Cr_{55}Al_{232-\delta}$ is comparatively stronger. Our resulting picture of $Cr_{55}Al_{232-\delta}$ is one in which strong bonding leads to local icosahedral units, which are in turn arranged into a large, complex unit cell.

We performed microhardness measurements to probe the nature of the strong hybridization inferred from our observation of short Cr-Al nearest-neighbor distances. Figure 2(a) provides an image of a microhardness indentation made at $T = 298$ K, for which a Vickers pyramidal diamond indenter was driven into the (001) face of a $Cr_{55}Al_{232-\delta}$ crystal with

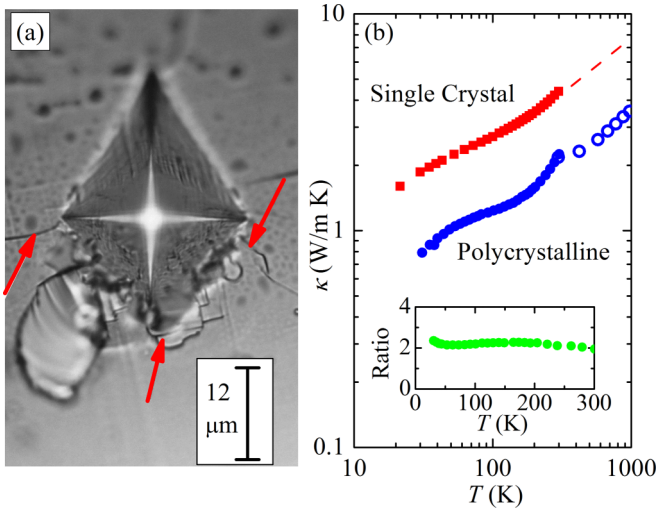

FIG. 2. (a) An optical microscope image of a microhardness indentation in the (001) face of a $Cr_{55}Al_{232-\delta}$ crystal. Fractures introduced during indentation are indicated by red arrows, and the average crack length is 52 μm. (b) The temperature dependence of the thermal conductivity κ of a single crystal (red solid squares) and a polycrystalline sample as determined by the steady state technique [30] (blue solid circles) and as calculated from thermal diffusivity measurements (blue open circles, see text). The inset shows the temperature dependence of the ratio of κ of the single crystal to that of the polycrystal.

force 2.94 N over a period of 15 s. The obtained hardness $H = 4.7 \pm 0.3$ GPa is high among Al-rich compounds and is similar to the value of hardened and tempered 4NiCrMo steel, an ultrahigh strength aircraft steel [35]. We note that the indentation in Fig. 2(a) is not perfectly symmetrical, despite the crystal surface lying flat to within 3°, an occurrence that is not entirely uncommon in single-crystal samples. The microhardness indentation initiated the propagation of several mode I (opening mode) cracks along the surface of the crystal, facilitating the estimation of mode I fracture toughness K_{IC} via the Evans and Charles equation $K_{IC} = 0.16(c/a)^{-1.5}(Ha^{1/2})$, where a is the average of the half lengths of the indentation diagonals and c is the average length the indentation fractures [36]. The obtained value of $K_{IC} \simeq 1.0\,\mathrm{MPa\,m^{1/2}}$ is comparable to that of concrete [37]. We stress that K_{IC} was obtained from a single crystal, in which typical toughening mechanisms such as deflection by secondary phases, bifurcation via grain boundaries, and meandering by pores are by definition absent [38,39]. Nonetheless, this combination of remarkably high hardness and modest fracture toughness is incompatible with metallic bonding and suggests that Cr-Al hybridization in $Cr_{55}Al_{232-\delta}$ is covalent and strongly directional in character [40].

Thermal conductivity measurements show that this complex, covalently bonded structure is highly effective at scattering thermal transport [Fig. 2(b)]. Below 300 K, measurements of the thermal conductivity κ were performed via the steady state technique on both a single crystal and on a cold-pressed, sintered pellet of powderized single crystals. Both samples exhibit a similar temperature dependence, but as expected, κ of the polycrystalline sample is ~50% lower due the presence of additional scattering mechanisms. We do not observe a pronounced umklapp peak at lower temperatures, even in the single crystal, and the temperature dependence is very similar to previous reports of Al-rich quasicrystalline phases [41], suggesting that equivalent scattering mechanisms are at play here.

Above 300 K, thermal diffusivity α was measured via the laser flash technique, but such measurements were possible only on the polycrystalline sample due to the size limitations of our crystal growth process. Here, we calculate $\kappa = \alpha\rho C_V$ for $T > 300$ K, where ρ is the measured mass density, and the heat capacity C_V was estimated from the Dulong-Petit limit. Aside from a slight radiation tail that appears above 250 K in the steady state data, there is excellent agreement between the two techniques and temperature regimes, and by $T = 1000$ K, κ reaches only 3.56 W/m K. Given that the ratio of κ between single-crystal and polycrystalline samples remains $\simeq$2 for all $T \leqslant 300$ K [Fig. 2(b), inset], we suggest a value of $\simeq$7 W/m K near 1000 K is likely for single-crystalline $Cr_{55}Al_{232-\delta}$. Such low values of κ tend only to be achievable with strong phonon-scattering properties of heavy elements or else when the electronic contribution to thermal conductivity is absent [42–44]. The electrical resistivity of $Cr_{55}Al_{232-\delta}$ increases with temperature (shown in SM [29]), however, indicating metallic behavior. Given that $Cr_{55}Al_{232-\delta}$ is neither heavy nor insulating, low κ here is likely a direct consequence of the crystal structure.

Figure 3 shows that $Cr_{55}Al_{232-\delta}$ exhibits excellent resistance to oxidation. In Fig. 3(a), we show the cross section of a single crystal cut and polished along the (001) direction after heat treatment of 1.09×10^6 s at 973 K in air. Two oxide layers are visible. An outer layer with EDX composition near Al_2O_3 exhibits a uniform thickness of 120 nm, while an inner layer with EDX composition near $Cr_{0.4}Al_{1.6}O_3$ varies

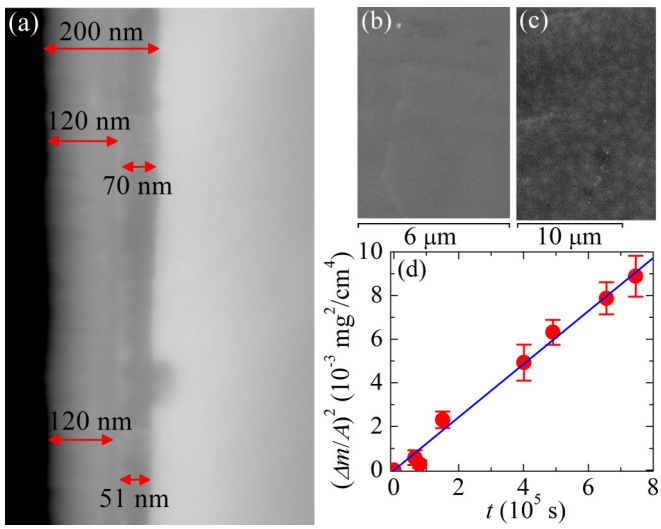

FIG. 3. SEM images of the (001) surface of a $Cr_{55}Al_{232-\delta}$ crystal (a) cut and polished to show the oxide cross section after 1.09×10^6 s at 973 K in air and eight thermal cycles to and from room temperature. The surface (b) as-grown and (c) after after oxidation. (d) The time t dependence of the square of the mass gain per unit area $(\Delta m/A)^2$ of a single crystal of $Cr_{55}Al_{232-\delta}$ as it is heated in air at 973 K. Data are shown in red, and the solid blue line is the best fit to the parabolic rate law. Error bars represent standard deviations in ten measurements of mass increase per t.

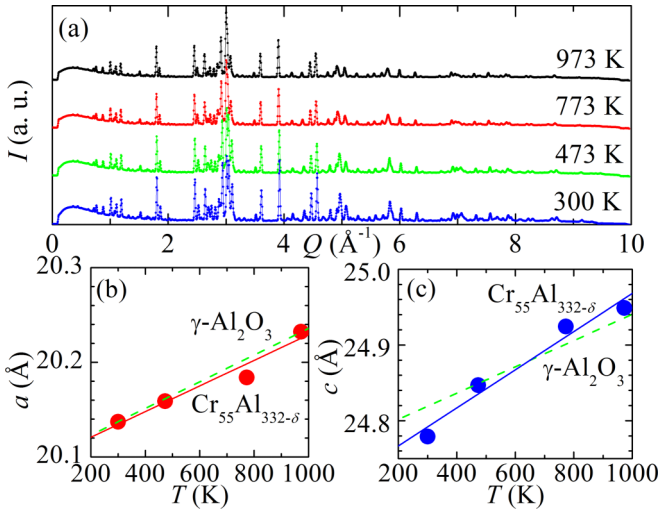

FIG. 4. (a) An overlay of powder x-ray diffraction measurements, plotted as a function of the magnitude of the scattering vector Q and performed at $T = 300$ K (blue), 473 K (green), 773 K (red), and 973 K (black) as indicated. The (b) a (red) and (c) c (blue) lattice parameters extracted from Le Bail refinement of the data shown in (a). Error bars are smaller than the size of the circles. Solid lines were determined by linear regression of the lattice parameter data to serve as a guide for the eye, and the slope of the green dashed line represents the thermal expansion coefficient of γ-Al_2O_3 for comparison [46].

from 50 to 70 nm. Figure 3(b) provides an SEM image of the smooth, nearly featureless (001) surface of an as-grown crystal of $Cr_{55}Al_{232-\delta}$, while Fig. 3(c) shows a speckled surface, revealing the formation of a fine scale with a characteristic size of $\sim$1 μm after the 1.09×10^6 s oxidation regimen. Despite eight thermal cycles from room temperature to 973 K and back, we observe no cracking or spallation of the scale.

The absence of scale cracking is consistent with our observation that $Cr_{55}Al_{232-\delta}$ oxidizes at a parabolic rather than linear rate. In Fig. 3(c), we plot as a function of time t the squared increase in mass of a single crystal due to oxidation in air at 973 K. Assuming uniform oxidation as observed via SEM, the mass increase after exposure for a period of 7.5×10^5 s corresponds to an Al_2O_3 scale thickness of 550 nm, in reasonable agreement with the thicknesses observed via cross sectioning. Mass increase permits calculation of the parabolic rate constant $k_p = (\Delta m/A)^2/t$, where $\Delta m/A$ represents the oxidative mass gain per unit area. The linear fit corresponds to $k_p = 1.2 \times 10^{-8}$ mg^2/cm^4 s, revealing excellent oxidation resistance compared to Cr-based compounds at this temperature, with k_p roughly a factor of 100 lower than is reported for MCrAlY (M = Co, Ni) coatings and 1000 times lower than Cr-Ni steels [45]. We place $Cr_{55}Al_{232-\delta}$ within the context of a wider range of high-temperature materials below.

To understand the structural origin of the oxide scale's robustness, we extended our diffraction measurements to higher temperatures. In Fig. 4(a), we plot an overlay of several patterns obtained from powderized single crystals. We observe no crystallographic phase transition, and the diffracted peaks remain sharp to the highest temperature measured, indicating that the structure remains stable to at least 973 K. As T is increased, the diffracted peaks shift to lower Q, signaling expansion of the lattice. In Figs. 4(b) and 4(c) we plot the a and c lattice parameters extracted from these data, both of which increase somewhat linearly over the investigated temperature range, yielding thermal expansion coefficients $\alpha_a = 6.72 \times 10^{-6}$ K^{-1} and $\alpha_c = 1.02 \times 10^{-5}$ K^{-1}, respectively. These values are in excellent agreement with the reported thermal expansion coefficient of γ-Al_2O_3, $\alpha_\gamma \simeq 7 \times 10^{-6}$ K^{-1} [46], which is the surface energy-stabilized polymorph favored in this temperature range [47]. Accordingly, we propose that the compatibility between the thermal expansion rates of Al_2O_3 and $Cr_{55}Al_{232-\delta}$ is one of the primary factors behind the robustness of the scale in the face of thermal cycling.

From this suite of measurements, we begin to formulate an understanding of the relationships between the structure and properties of $Cr_{55}Al_{232-\delta}$. Diffraction and hardness measurements together reveal a rigid material in which the

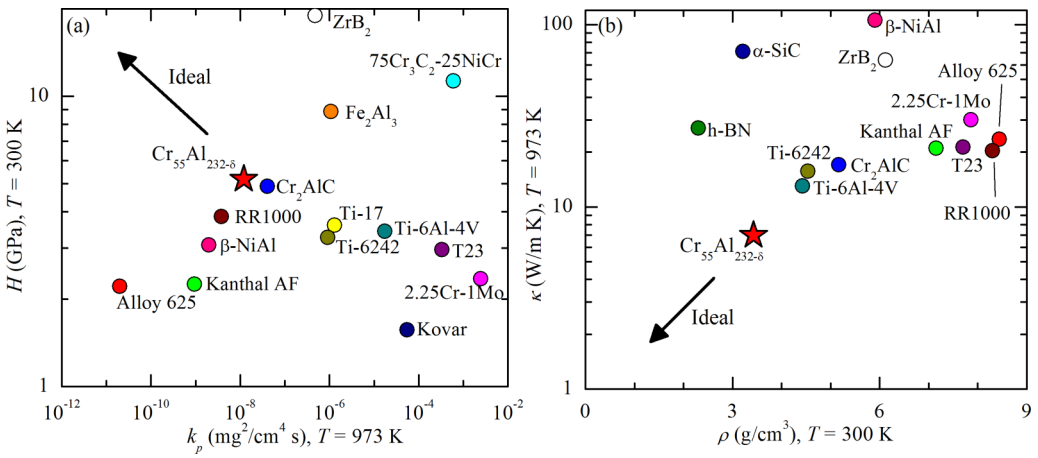

FIG. 5. Surveys of the (a) hardness H (vertical axis) vs parabolic rate constant k_p (horizontal axis) and (b) thermal conductivity κ (vertical axis) vs mass density ρ (horizontal axis) of $Cr_{55}Al_{232-\delta}$ (red star) as well as a selection of refractory compounds and alloys, including the following: Alloy 625 (red) [48,49], h-BN (green) [50], Cr_2AlC (blue) [51,52], $75Cr_3C_2$-25NiCr (cyan) [17,53], 2.25Cr-1Mo (magenta) [17,54,55], Fe_2Al_3 (orange) [56,57], Kanthal AF (green) [58,59], Kovar (dark blue) [60], β-NiAl (pink) [61–63], RR1000 (brown) [64,65], α-SiC (indigo) [66–68], T23 (purple) [69], Ti-17 (yellow) [70,71], Ti-6242 (gold) [70,71], Ti-6Al4V (teal) [72,73], and ZrB_2 (white) [74–76], as indicated.

crystal structure is determined by strong nearest-neighbor bonding with predominantly covalent character. According to this picture, the competition between energy scales associated with directional covalent bonding and those associated with efficient packing underscores the opposition of long-range hexagonal and short-range icosahedral symmetries and is ultimately responsible for the large and complex unit cell, as well as the high resistance to thermal transport.

Figure 5 places the properties of $Cr_{55}Al_{232-\delta}$ within the context of a variety of well-studied, oxidation-resistant refractory materials, including steels, titanium alloys, chromium alloys, aluminides, borides, and carbides. In Fig. 5(a) we compare hardness H at 300 K with the parabolic oxidation rate coefficient k_p in air at 973 K. While it would be preferable to compare values of H determined at expected operating temperatures, such data are presently unavailable on a wide range of materials due to the requirement for specialized instrumentation. While $Cr_{55}Al_{232-\delta}$ is neither the hardest nor most oxidation-resistant compound plotted, in the context of existing materials it is both hard for one so oxidation resistant and oxidation resistant for one so hard, striking a balance between these two critical properties. Figure 5(b) compares thermal conductivity κ at 973 K with mass density ρ. Here, $Cr_{55}Al_{232-\delta}$ is unique in its low κ, particularly for a material so light. Even covalent materials of comparable ρ such as BN and SiC are several times less thermally insulating, while the majority of high-temperature alloys and steels are both substantially denser and less thermally insulating. Placed within this context, our measurements of high hardness, low thermal conductivity, and excellent oxidation resistance suggest that $Cr_{55}Al_{232-\delta}$ may be well suited for high-temperature applications.

Because these properties are largely underpinned by the local icosahedral character of the structure, we suggest they may be a general feature of Al-based pseudo-icosahedral compounds. Many such compounds are already known in the crystallographic literature, providing a rich field from which relevant properties might be more perfectly optimized. For instance, while the hardness of $Cr_{55}Al_{232-\delta}$ is unparalleled among Cr-Al compounds, fracture toughness remains modest. We point out that our measurement of H was performed at $T = 298$ K, and it is likely that ductility will increase with T, resulting in enhanced fracture toughness at elevated temperatures. The existence of a ductile-brittle transition appears to be a general feature of Al-based icosahedral compounds [40] and is intimately related to the number of valence electrons of transition-metal constituents, with their contribution to the Al-based skeleton serving to stabilize the electronic structure. The close relationship between valence electron count and the ductile-brittle criterion suggests that optimal toughness at 973 K may be achievable via compositional tuning in the form of $Cr_{55-x}M_xAl_{232-\delta}$, for heterovalent transition-metal M.

Similarly, the robust oxidation resistance appears to be the direct result of both high Al content and the fortuitous compatibility between the thermal expansion of $Cr_{55}Al_{232-\delta}$ and that of Al_2O_3 scale uniformly distributed across its surface. Given that Hume-Rothery stabilization is crucial to determining the electronic structure of icosahedral Al-based compounds [77], we posit that thermal expansion likewise could be more precisely tuned via small compositional modifications performed with an eye towards varying the number of valence electrons.

The compatibility of $Cr_{55}Al_{232-\delta}$-derived materials with various deposition techniques must also be addressed. Fortunately, the deposition of Al-rich transition-metal coatings is already an established field and can be accomplished via a number of processes [12–20], suggesting that realizing such compounds in coating form may be feasible. For large-scale infrastructure projects associated with electrical power generation, economic feasibility requires a demanding set of criteria, but $Cr_{55}Al_{232-\delta}$ is of low density and can be synthesized via an exposed liquidus at relatively low temperatures from inexpensive metals, suggesting that commercialization may prove in the end to be economical.

Acknowledgment is made to the Donors of the American Chemical Society Petroleum Research Fund, for support of this research under Contract No. 56764-UNI10. This research used resources of the Center for Functional Nanomaterials, which is a U.S. DOE Office of Science Facility, at Brookhaven National Laboratory under Contract No. DE-SC0012704. Use of the National Synchrotron Light Source II, Brookhaven National Laboratory, was supported by the U.S. Department of Energy, Office of Science, Office of Basic Energy Sciences, under Contract No. DE-SC0012704. Work at Texas A&M University was supported by the Welch Foundation, Grant No. A-1890-20160319. The Stony Brook University single-crystal diffractometer was obtained through the support of the National Science Foundation Grant No. CHE-0840483. R.R. was supported by an NYSED CSTEP Grant, under Contract No. C401633. J.W.S. was supported in part by a Provost's Research Fellowship from Farmingdale State College. We thank Y. Janssen for his constructive comments on the manuscript.

[1] L. Irwin and Y. L. Moullec, Science **356**, 805 (2017).
[2] R. J. Campbell, Congressional Research Service Report No. 7-5700, 2013, https://fas.org/sgp/crs/misc/R42923.pdf.
[3] F. Abe, Curr. Opin. Solid State Mater. Sci. **8**, 305 (2004).
[4] X. Zhang, Q. Yan, Y. Yang, Z. Hong, L. Zhang, and C. Ge, Corrosion **71**, 50 (2015).
[5] S.-H. Kim, H. Kim, and N. J. Kim, Nature (London) **518**, 77 (2015).
[6] Q. Lu, W. Xu, and S. van der Zwaag, Acta Mater. **77**, 310 (2014).
[7] Q. Lu, W. Xu, and S. van der Zwaag, Acta Mater. **64**, 133 (2013).
[8] M. Taneike, F. Abe, and K. Sawada, Nature (London) **424**, 294 (2003).
[9] Z. B. Jiao, J. H. Luan, Z. W. Zhang, M. K. Miller, W. B. Ma, and C. T. Liu, Acta Mater. **61**, 5996 (2013).
[10] S. Tang, S. Zhu, X. Tang, H. Pan, X. Chen, and Z. D. Xiang, Corros. Sci. **80**, 374 (2014).

[11] Z. Liu, Y. Gong, W. Zhou, L. Ma, J. Yu, J. C. Idrobo, J. Jung, A. H. MacDonald, R. Vajtai, J. Lou, and P. M. Ajayan, Nat. Commun. **4**, 2541 (2013).

[12] B. L. Bates, Y. Q. Wang, Y. Zhang, and B. A. Pint, Surf. Coat. Technol. **204**, 766 (2009).

[13] Z. D. Xiang, D. Zeng, C. Y. Zhu, S. R. Rose, and P. K. Datta, Corros. Sci. **53**, 496 (2011).

[14] B. A. Pint, Y. Zhang, L. R. Walker, and I. G. Wright, Surf. Coat. Technol. **202**, 637 (2007).

[15] S. Velraj, Y. Zhang, E. W. Hawkins, and B. A. Pint, Mater. Corros. **63**, 909 (2012).

[16] V. Rohr and M. Schutze, Surf. Eng. **20**, 266 (2004).

[17] D. Ghosh and S. K. Mitra, Surf. Eng. **31**, 342 (2015).

[18] Z. D. Xiang, S. R. Rose, P. K. Datta, and M. Scheeffer, Surf. Coat. Technol. **203**, 1225 (2009).

[19] W. Li, J. Cai, and G. Ling, Acta. Metall. Sin. **47**, 231 (2011).

[20] M. Zhang, B. Xu, and G. Ling, Appl. Surf. Sci. **331**, 1 (2015).

[21] B. Grushko, B. Przepiórzyński, E. Kowalska-Strzęciwilk, and M. Surowiec, J. Alloys Compd. **420**, L1 (2006).

[22] H. Wu, M. Zhang, B. Xu, and G. Ling, J. Alloys Compd. **610**, 492 (2014).

[23] M. Audier, M. Durand Charre, E. Laclau, and H. Klein, J. Alloys. Compd. **220**, 225 (1995).

[24] S. Kamal, R. Jayaganthan, S. Prakash, and S. Kumar, J. Alloys. Compd. **463**, 358 (2008).

[25] C. B. Shoemaker, Phys. Rev. B **38**, 8511(R) (1988).

[26] C. B. Shoemaker, D. A. Keszler, and D. P. Shoemaker, Acta Crystallogr., Sect. B **45**, 13 (1989).

[27] B. B. Cao and K. H. Kuo, J. Alloys Compd. **458**, 238 (2008).

[28] B. B. Cao, J. Alloys Compd. **698**, 605 (2017).

[29] See Supplemental Material at http://link.aps.org/supplemental/10.1103/PhysRevMaterials.2.032401 for details regarding crystal structure solution and electric and thermal transport measurements.

[30] A. L. Pope, B. Zawilski, and T. M. Tritt, Cryogenics **41**, 725 (2001).

[31] P. Sarin, W. Yoon, K. Jurkschat, P. Zschack, and W. M. Kriven, Rev. Sci. Instrum. **77**, 093906 (2006).

[32] D. Levine and P. J. Steinhardt, Phys. Rev. B **34**, 596 (1986).

[33] J. Braun, M. Ellner, and B. Predel, J. Alloys Compd. **183**, 444 (1992).

[34] A. Kallel, Compt. Rend. Acad. Sci. Paris B **268**, 455 (1969).

[35] D. L. Porter and T. C. Totemeier, *Smithells Metals Reference Book*, 8th ed. (Elsevier, Oxford, UK, 2004).

[36] A. G. Evans and E. A. Charles, J. Am. Ceram. Soc. **59**, 371 (1976).

[37] S. A. Hamoush and H. Abdel-Fattah, Eng. Frac. Mech. **53**, 425 (1996).

[38] F. Bouville, E. Maire, S. Meille, B. Van de Moortèle, A. J. Stevenson, and S. Deville, Nat. Mater. **13**, 508 (2014).

[39] S. G. Isaacson, K. Lionti, W. Volksen, T. P. Magbitang, Y. Matsuda, R. H. Dauskardt, and G. Dubois, Nat. Mater. **15**, 294 (2016).

[40] H. Niu, X.-Q. Chen, P. Liu, W. Xing, X. Cheng, D. Li, and Y. Li, Sci. Rep. **2**, 718 (2012).

[41] A. L. Pope, T. M. Tritt, M. A. Chernikov, and M. Feuerbacher, Appl. Phys. Lett. **75**, 1854 (1999).

[42] L. Zhou, P. Qiu, C. Uher, X. Sun, and L. Chen, Intermetallics **32**, 209 (2013).

[43] D. R. Clarke and S. R. Phillpot, Mater. Today **8**, 22 (2005).

[44] A. van Roekeghem, J. Carrete, C. Oses, S. Curtarolo, and N. Mingo, Phys. Rev. X **6**, 041061 (2016).

[45] Y. Lu, W. Chen, and R. Eadie, Intermetallics **12**, 1299 (2004).

[46] N. N. Ault, J. Am. Ceram. Soc. **40**, 69 (1957).

[47] J. M. McHale, A. Auroux, A. J. Perrotta, and A. Navrotsky, Science **277**, 788 (1997).

[48] H. Buscail, R. Rolland, C. Issartel, F. Rabaste, F. Riffard, L. Aranda, and M. Vilasi, J. Mater. Sci. **46**, 5903 (2011).

[49] L. Garcia-Fresnillo, A. Chyrkin, C. Böhme, J. Barnikel, F. Schmitz, and W. J. Quadakkers, J. Mater. Sci. **49**, 6127 (2014).

[50] A. Simpson and A. D. Stuckes, J. Phys. C **4**, 1710 (1971).

[51] W. Tian, P. Wang, G. Zhang, Y. Kan, Y. Li, and D. Yan, Scr. Mater. **54**, 841 (2006).

[52] D. B. Lee, T. D. Nguyen, and S. W. Park, Oxid. Met. **77**, 275 (2012).

[53] A. Özer and Y. K. Tür, Bull. Mater. Sci. **36**, 907 (2013).

[54] S. A. Kamal, C. W. Grandy, M. T. Farmer, and A. R. Brunsvold, Argonne National Laboratory Technical Report No. ANL-04/27, (2004).

[55] H. Kushima, T. Watanabe, M. Murata, K. Kamihira, H. Tanaka, and K. Kimura, in *Creep and Fracture in High Temperature Components: Design and Life Assessment Issues*, edited by I. A. Shibli, S. R. Holdsworth, G. Merckling, and European Creep Collaborative Committee (DEStech Publications, Lancaster, PA, 2005), p. 223.

[56] M. Badaruddin, S. Suharno, and H. A. Wijaya, J. Teknik Mesin **15**, 15 (2014).

[57] P. Matysik, S. Jóźwiak, and T. Czujko, Materials **8**, 914 (2015).

[58] H. Josefsson, F. Liu, J.-E. Svensson, M. Halvarsson, and L.-G. Johansson, Mater. Corros. **56**, 801 (2005).

[59] Kanthal AF Strip Datasheet, Kanthal, Hallstahammar, Sweden, 19 January 2017.

[60] J. J. Stephens, F. A. Greulich, and L. C. Beavis, High temperature grain growth and oxidation of Fe-29Ni-17Co (Kovar^{TM}) alloy leads, Sandia National Laboratory No. SAND-93-2168C, CONF-9211117-12, 1993.

[61] J. T. Guo and Z. P. Xing, J. Mater. Res. **12**, 1083 (1997).

[62] H. J. Grabke, Intermetallics **7**, 1153 (1999).

[63] Y. Terada, K. Ohkubo, T. Mohri, and T. Suzuki, Intermetallics **7**, 717 (1999).

[64] R. J. Mitchell, M. Preuss, S. Tin, and M. C. Hardy, Mater. Sci. Eng., A **473**, 158 (2008).

[65] A. Encinas-Oropesa, G. L. Drew, M. C. Hardy, A. J. Leggett, J. R. Nicholls, and N. J. Simms, Superalloys **2008**, 609 (2008).

[66] T. Narushima, T. Goto, T. Hirai, and Y. Iguchi, Mater. Trans., JIM **38**, 821 (1997).

[67] St. G. Müller, R. Eckstein, J. Fricke, D. Hofmann, R. Hofmann, R. Horn, H. Mehling, and O. Nilsson, Mater. Sci. Forum **264–268**, 623 (1998).

[68] Yu. V. Milman, S. I. Chugunova, I. V. Goncharova, T. Chudoba, W. Lojkowski, and W. Gooch, Int. J. Refract. Hard Met. **17**, 361 (1999).

[69] S.-H. Bak, M.-J. Kim, J.-H. Lee, S.-J. Bong, S.-K. Kim, and D.-B. Lee, J. Korean Ceram. Soc. **48**, 57 (2011).

[70] A. Ebach-Stahl, C. Eilers, N. Laska, and R. Braun, Surf. Coat. Technol. **223**, 24 (2013).

[71] *Materials Properties Handbook: Titanium Alloys*, edited by R. Boyer, G. Welsch, and E. W. Collings (ASM International, Materials Park, OH, 1994).

[72] M. Boivineau, C. Cagran, D. Doytier, V. Eyraud, M.-H. Nadal, B. Wilthan, and G. Pottlacher, Int. J. Thermophys. **27**, 507 (2006).
[73] H. Guleryuz and H. Cimenoglu, J. Alloys Compd. **472**, 241 (2009).
[74] J. W. Zimmermann, G. E. Hilmas, and W. G. Fahrenholtz, J. Am. Ceram. Soc. **91**, 1405 (2008).
[75] W.-M. Guo, G.-J. Zhang, Y.-M. Kan, and P.-L. Wang, J. Alloys Compd. **471**, 502 (2009).
[76] M. S. Asl, M. G. Kakroudi, and S. Noori, J. Alloys Compd. **619**, 481 (2015).
[77] G. Trambly de Laissardière, D. Nguyen-Manh, and D. Mayou, Prog. Mater. Sci. **50**, 679 (2005).